Citric Acid Based Carbon Dots with Amine Type Stabilizers: pH-specific Luminescence and Quantum Yield Characteristics

Florian Meierhofer,[†a] Frank Dissinger,[‡a] Florian Weigert,[§] Jörgen Jungclaus,[†] Knut Müller-Caspary,[⊥] Siegfried R. Waldvogel,[‡] Ute Resch-Genger,[*,§] Tobias Voss*[,†]

[†]Institute of Semiconductor Technology and Laboratory for Emerging Nanometrology (LENA), TU Braunschweig, 38106 Braunschweig, Germany
[‡]Institute of Organic Chemistry, Johannes Gutenberg University, 55128 Mainz, Germany
[§]BAM- Federal Institute for Materials Research and Testing, Division 1.10 Biophotonics, 12489 Berlin, Germany
[⊥]Ernst Ruska-Centre for Microscopy and Spectroscopy with Electrons, Forschungszentrum Jülich, 52425 Jülich, Germany

Corresponding Author

*E-Mail: tobias.voss@tu-braunschweig.de, ute.resch@bam.de
[a] These authors contributed equally to this work.

Abstract

We report the synthesis and spectroscopic characteristics of two different sets of carbon dots (CDs) formed by hydrothermal reaction between citric acid and polyethylenimine (PEI) or 2,3-diaminopyridine (DAP). Although the formation of amide-based species and the presence of citrazinic acid type derivates assumed to be responsible for a blue emission is confirmed for both CDs by elemental analysis, infrared spectroscopy, and mass spectrometry, a higher abundance of sp^2-hybridized nitrogen is observed for DAP-based CDs, which causes a red-shift of the n-π^* absorption band relative to the one of PEI-based CDs. These CD systems possess high photoluminescence quantum yields (QY) of ~40% and ~48% at neutral pH, demonstrating a possible tuning of the optical properties by the amine precursor. pH-dependent spectroscopic studies revealed a drop in QY to <9% (pH ~1) and <21% (pH ~12) for both types of CDs under acidic and basic conditions. In contrast, significant differences in the pH-dependency of the n-π^* transitions are found for both CD types which are ascribe to different (de-)protonation sequences of the CD-specific fluorophores and functional groups using zeta potential analysis.

1. Introduction

The discovery of light emission from carbon dots (CDs)[1,2] has triggered an enormous interest to develop the next-generation of carbon-based photonic and optoelectronic materials with the ultimate goal to eventually replace traditional inorganic semiconductor quantum dots (QDs) like II/VI QDs that contain toxic heavy metal ions (*e.g.* Cd^{2+}, Pb^{2+}, *etc*.).[3–7] Advantages of CDs are their ease of fabrication ("green synthesis") from low-cost precursors consisting of earth-abundant elements (*e.g.* carbon, nitrogen, oxygen, *etc*.), environmental-friendliness, good biocompatibility, and high photostability. The synthesis of CDs either relies on top-down or bottom-up strategies.[8–11] Among the latter, the hydrothermal synthesis is one of the most frequently used methods that allows tuning of the optical characteristics of the resulting CDs by variation of the applied precursors and/or synthesis conditions.[12–15]

The generally accepted model for the structure of the CDs assumes the existence of an sp^2 hybridized carbon core which is embedded in an sp^3 hybridized carbon matrix with additional surface functional groups (*e.g.* hydroxyl, carboxyl, epoxy, amino, amides, *etc*., **Scheme 1**). The chemical nature of the latter depends on the individual precursors, synthesis conditions (temperature, time, solvent, pH, reactant ratio, *etc*.), and subsequent purification procedures, such as column chromatography, centrifugation, dialysis *etc*.[16–19] Particularly the use of nitrogen containing precursors can affect the characteristic light emission and quantum yield (QY) of the resulting CDs.[20–23] An attractive feature, that is often observed for CDs, is the excitation-wavelength dependent photoluminescence (PL) which implies that the emission wavelength and intensity can be altered by changing the excitation wavelength. Several explanations for the PL of CDs have been reported, ranging from electronic transitions inside the quantum-confined carbon core, contribution of surface trap states, and/or the existence of (multi-)chromophores/fluorophores within single particles.[21,24–32]

The electronic transitions involved in the luminescence of CD solutions are directly affected by the respective surface groups and surface bound fluorophores and their interaction with the CD microenvironment. Recently, a solvatochromic behavior of CDs without[33,34] and with nitrogen-doping[11,35] has been reported, resulting in a bathochromic shift of the emission maximum with increasing solvent polarity.[35] Moreover, in protic solvents this red-shift in emission is enhanced compared to aprotic solvents with similar dielectric constants, thereby indicating contributions of hydrogen-bond interactions between CD surface groups/states and the solvent.[35] This was confirmed by studies of the influence of pH on the optical properties of CDs obtained without[16,17,30,36–42] or with nitrogen containing precursors,[21,22,43–60] where changes from acidic to basic conditions affected the PL intensity and/or shifted the PL bands to lower or higher energies. Such changes in PL might originate from protonation or deprotonation of specific CD surface groups like amine functionalities.[17,52] Despite several studies, these effects are still not well understood.

In this work, we describe the structure and spectroscopic properties of two nitrogen-doped sets of CDs which were formed during the reaction between citric acid (CA) and polyethylenimine (PEI) or 2,3-diaminopyridine (DAP) within the course of a hydrothermal synthesis. We also assessed the pH-dependence of the absorption and luminescence properties of both CD systems. These studies demonstrate that the choice of the amine precursor presents a key for tuning the spectral position of the CD absorption bands and optical transitions responsible for an intense PL with a high QY. Moreover, we show that

the PL of these CDs is closely related to a sequence of (de-)protonation steps of the CD surface functional groups and the CD-specific fluorescent moieties introduced via the nitrogen-containing precursors that are suggested by MS data.

2. Experimental Section

2.1. CD synthesis. The synthesis of the studied CDs is illustrated in **Scheme 1** and is based on previously established hydrothermal synthesis protocols.[55,61–63] In particular, CA as a carbon source in combination with PEI or DAP as nitrogen sources are treated hydrothermally to form two different types of CDs. The systems obtained from CA/PEI and CA/DAP are referred to as “CD1“ and “CD2“ in the following. These amine precursors were chosen as they are supposed to form different chemical structures during the hydrothermal synthesis leading to different optical properties of the respective carbon dots. In order to obtain CDs with high QY, a comparably short reaction time (45 min) was used.[18] Further details of the synthesis are provided in the **Supporting Information** (SI, section S1) and in **Table S1**. During the hydrothermal synthesis, amides and fluorophore intermediates are initially formed by dehydration, which are then carbonized within the course of the reaction.[18,64] These fluorophores remain on the particle surface even after carbonization[65] and can be bound to the particle surface adsorptively or covalently. The surface of the resulting two types of CDs is assumed to bear different functional groups (*e.g.* carboxyl, hydroxyl, amides, *etc*.) which remain from the reaction as well as the different fluorophore moieties as shown in **Scheme 1**. The condensation reaction between CA and PEI should lead to pyridine-type fluorophores. As PEI partly decomposes to ammonia during the reaction, this can lead to the formation of citrazinic acid, similar to experiments using urotropine as amine compound.[66] Furthermore, pyridine-type structures, similar to the recently published fluorophore 5-oxo-1,2,3,5-tetrahydroimidazo[1,2-α]pyridine-7-carboxylic acid (IPCA) could be formed.[66] As IPCA is synthesized using ethylene diamine, the formation of similar structures is, in our case, constrained to the branches bearing primary amine groups, as the main polymer chain of PEI consists of only secondary or tertiary amines. The fluorophores at the surface of CD1 could also consist of citrazinic acid-type derivatives with a PEI substituent. These moieties contain solely aliphatic amine functions which might all be protonated yielding aliphatic $NR_{(1-3)}H_{(3-1)}^{+}$ groups at a similar pKa of ~9. In contrast, selecting an amine precursor that already contains aromatic nitrogen like DAP should lead to CDs with a higher percentage of sp^2-hybridized (graphitic) nitrogen. The influence of this aromatic nitrogen content has been reported to play a major role in the luminescence characteristics of CDs.[67] As DAP contains the aromatic heterocycle pyridine and two attached aniline functions with pKa values of ~4, the basicity of CD2 is significantly lower compared to PEI, and, hence, also lower compared to the PEI-containing CD1.[68,69] Additionally, a protonation of the pyridine moiety directly influences the aromatic π-system that mainly determines the photophysical properties. More importantly, the aromatic *ortho*-amines of DAP are perfectly suited to form either citrazinic acid-type structures, or after a second condensation even carbazole-type fluorophores both with delocalized π-systems that are expected to bathochromically shift the absorption bands of CD2. These fluorescent molecules, that could be present on the surface of CD2, should feature three main functionalities, i.e., a carboxyl function and secondary and tertiary amino groups. This is expected to result in clearly different pH dependent characteristics of CD1 and CD2.

2.2. Characterization of CDs and precursor materials. *Transmission Electron Microscopy (TEM)* characterization was performed at a FEI Titan 80/300 (S)TEM facility equipped with an aberration corrector for the imaging system. An aliquot of the aqueous CD solution was sonicated and placed on a carbon coated copper grid and air-dried prior loading the sample into the microscope which was operated at 300 kV acceleration voltage. A Gatan UltraScan 1000 slow-scan charge-coupled device (CCD) was used to record TEM images with exposure times between 0.1 and 1 s at slight under-focus. Elemental composition of CDs was quantified by using a scanning electron microscope (SEM, Zeiss EVO MA 25) equipped with an *energy dispersive X-ray spectroscopy (EDX)* unit (AMETEK, Apollo X). Agglomerated clusters of freeze-dried CDs were attached to the edges of a carbon sticking tape to gain a signal solely from the sample (and not from the carbon tape). The samples were tilted to a 30 ° angle and the SEM was operated at 5 kV acceleration voltage (~10 mm working distance, 200x magnification, 2000 nA cathode current), while the EDX spectrum was obtained after 30 s of integration. *Fourier-transform infrared* (FTIR, Jasco FV 6700 IR) spectroscopy was performed by pressing dry CD powders to an attenuated total reflection (ATR) diamond window (GladiATR, Pike). The spectra were obtained with a scan resolution of 4 cm^{-1} and by averaging 64 single scans for each sample. *HPLC-Mass spectra* were obtained using a G6545A Q-ToF (Agilent GmbH) with ESI ionization coupled to a 1260 Infinity II HPLC-System (Agilent GmbH). Eluent separation was performed using an Agilent Poroshell 120 EC-C18 column. 2 mg of respective crude CDs were dissolved in 1 mL methanol and 0.005 mL formic acid under sonication. 0.01 mL were then diluted in 1 mL of a methanol/water (90/10) mixture and injected into the HPLC-MS setup.

2.3. Characterization of CD solutions. The *UV-vis absorption* spectra of the dissolved CDs were measured in 10 mm quartz cuvettes (Helma GmbH) using a Specord Plus by Analytik Jena spectrometer with a resolution of 1 nm. *Absolute quantum yield (QY)* measurements were carried out with the calibrated integrating sphere setup Quantaurus-QY from Hamamatsu previously evaluated by Würth *et al*.[70] using long neck quartz cells from Hamamatsu (10 mm optical path). The absorbance at the excitation wavelength had to be kept below 0.01, thereby minimizing inner filter effects and reabsorption which could lead to an underestimate of PL QY. The zeta potential *(ZP)* was determined using a Zetasizer Nano instrument (Malvern Instruments, Worcestershire, UK) equipped with a 633 nm He–Ne laser at a scattering angle of 173° (backscatter) using the “General purpose” analysis model and the default size analysis parameters. Electrophoretic mobility of each sample was measured in low volume quartz cuvettes at room temperature. The Zeta potentials were then calculated by applying the Smoluchowski relation, which is valid for aqueous solutions containing low electrolyte concentrations. An average of three measurements per pH value was considered for each sample.

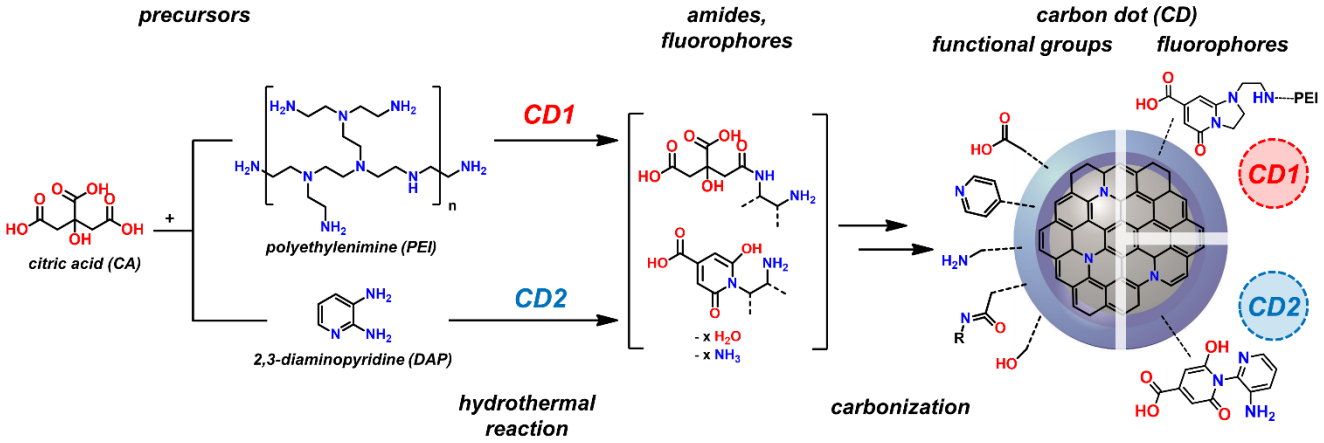

Scheme 1. CD1 and CD2 are obtained by solvothermal pyrolysis of citric acid (CA) with amine precursors PEI and DAP, respectively. During the reaction, amide bonds and carbonization reactions are conceived to affect the surface chemistry of the CDs. The selection of amine precursor directly affects the occurrence and number of functional groups and fluorescent moieties (fluorophores) in the CD products CD1 and CD2 and at their surface, thereby changing their optical properties and their response to pH changes.

3. Results and Discussion

3.1. Morphology, elemental, and chemical composition of the CDs. Transmission electron microscopy (TEM) of CD1 (**Figure 1a**) reveals the formation of non-spherical particles with an average projected area equivalent diameter (d_{avg}) of 10.5±2.9 nm. This diameter is in the same order of magnitude as reported in other studies.[67] Moreover, high-resolution (HR-) TEM indicates a partially ordered internal structure of the CDs (**Figure 1b**) due to the presence of crystal fringes with ~0.2 nm lattice spacing which are ascribed to the (100) plane of the graphitic crystal lattice.[8,67]

Energy dispersive X-ray (EDX) spectroscopy (**Figure 1c**) of CD-CA/PEI and CA/DAP shows bands at about 0.27, 0.39 and 0.53 keV attributed to K_α radiation of carbon (C), nitrogen (N) and oxygen (O), respectively. In both CDs, carbon has the largest elemental fraction (~58 and ~60 atom%), while nitrogen (~11 and ~9 atom%) and oxygen (~16 and ~17 atom%) constitute lower fractions suggesting successful reaction between CA (oxygen source) and amine precursor (nitrogen source). Moreover, we observed that the use of hydrochloric acid as an eluent for the purification of CD1 by column chromatography causes an increase in chlorine content (~12 % for CD1). This is confirmed by comparison to the non-purified product "CD1 (crude)". This modification apparently did not affect the fluorophore structure and the optical properties of CD1 or CD2 (more details are provided in the **SI**, section S7).

In order to provide more insight into the chemical nature of the CDs and their surface chemistry, Fourier-transform infrared (FTIR) spectra of CD1 and CD2 were measured and compared to those of the precursor molecules (**Figure 1d**, **1e** and **Table S3** in **SI** section S2). For CD1, broad absorption bands at ~3600–2300 cm^{-1} are observed that are ascribed to vibrational stretching of O-H, N-H and C-H groups. The signal width presumably originates from hydrogen bonds between individual CDs since the IR spectra were recorded for spray-dried (agglomerated) CDs. The relatively strong stretching signal at 1694 cm^{-1} suggests amide formation C(=O)(-NH), most likely resulting from the reaction between the carboxylic acid groups of CA (1721 and 1685 cm^{-1}) and the amine groups of PEI (1592 cm^{-1}). The

extended shoulder at 1638 cm^{-1} is attributed to the stretching vibrations of C=C and/or C=N groups and the existence of aromatic domains in CD1. The two peaks at 1553 and 1393 cm^{-1} are associated with asymmetric and symmetric stretching of carboxylate groups presumably remaining on the CD surface as derivates of the CA precursor.[40,71] The IR finger-print region of the CD shows up as a large background with some spectral overlap/crosstalk with other signals. This underlines the complex chemical structure of the CDs. The most dominant band is detected at 1179 cm^{-1} indicating the presence of phenolic hydroxyl groups (C-OH) that enhance the water-solubility of the CDs.[17,72]

In contrast to PEI, the IR spectrum of the amine precursor DAP (**Figure 1e**) features multiple vibrational peaks (1469, 1455, 1577, and 1597 cm^{-1}) that are indicative of C=C and C=N bonds in aromatic ring structures.[73,74] Therefore, the product CD2 reveals some differences compared to CD1 in particular for the amide bonds (1712 cm^{-1}), the sp^2-hybridized carbon bonds C=C and C=N (1659 cm^{-1}), and the asymmetric and symmetric vibrations originating from the carboxylates (1570 and 1384 cm^{-1}). The broad absorption bands attributed to O-H, N-H, C-H (3600-2300 cm^{-1}) and phenolic -OH (1179 cm^{-1}) groups are also obtained for CD2, suggesting that its chemical structure is still comparable to that of CD1.

To search for soluble fluorophores within the CD samples, as proposed by the literature[65,66,75,76], HPLC-MS measurements of the crude products were performed (section S3 in **SI**, **Figure S1**). For both samples, m/z ratios with higher molecular weight compared to the precursors could be obtained. In case of CD1, the spectra show a repetitive pattern that might origin from citrazinic acid type derivatives, functionalized with PEI moieties at the pyridine nitrogen. As no traces of non-functionalized citrazinic acid (m/z 155) or its amide (m/z 154) could be observed, a reaction pathway based on ammonia from degraded PEI is rather unrealistic. The m/z ratios of CD2 suggest the occurrence of citrazinic-type fluorophores with DAP as substituent could be identified, while any further condensation reaction towards IPCA-type fluorophores could not be observed (**SI**, **Scheme S1**).

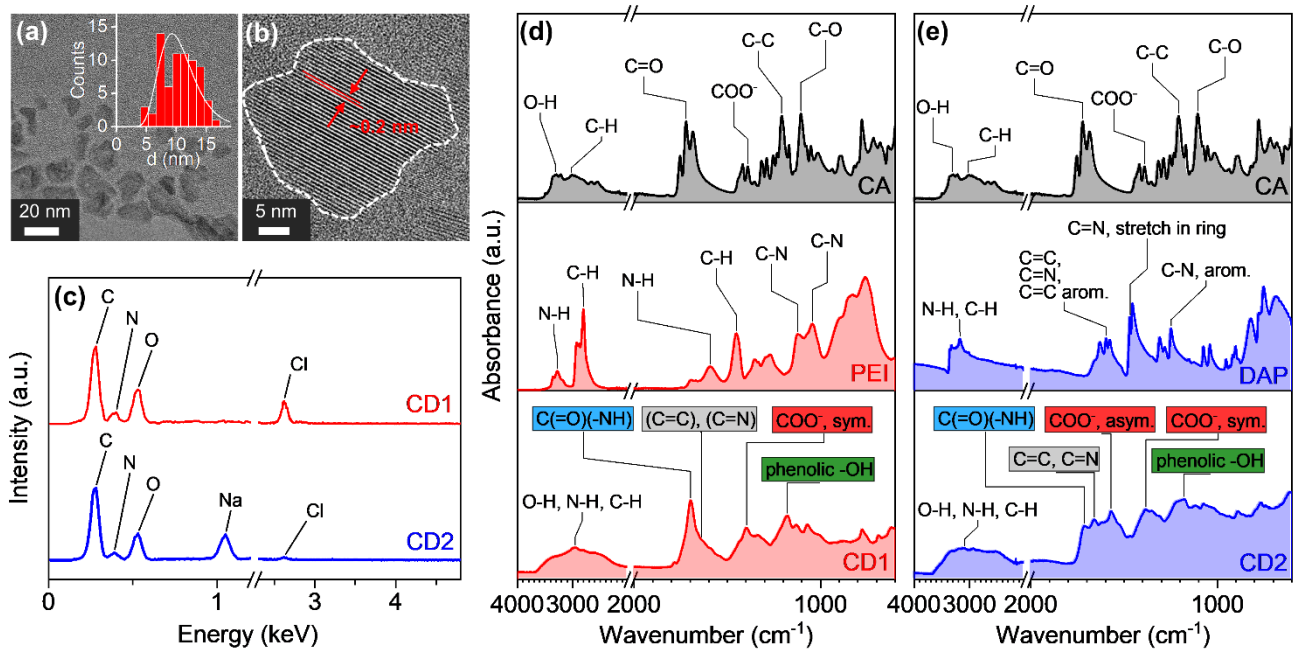

Figure 1. (a) TEM (the inset shows the projected-area diameter distribution with an average diameter d_{avg} of 10.5 nm and a standard deviation σ of 2.9 nm); **(b)** HRTEM imaging of CD1 indicate non-spherical particles with sizes around 10 nm and ordered internal graphitic structures; **(c)** EDX spectra of spray-

dried CDs revealing the elemental composition of CD1 (C 58.4 atom%, N 10.5 atom%, O 15.8 atom%, Cl 12.1 atom%, others 3.2 atom%) and CD2 (C 59.5 atom%, N 8.8 atom%, O 16.9 atom%, Na 10.8 atom%, Cl 1.9 atom%, others 2.1 atom%); **(d)** and **(e)** FTIR spectra of citric acid (CA), the amine precursor PEI and DAP, and the as-synthesized products CD1 and CD2.

3.2. Concentration-dependent optical properties of CDs. Excitation at λ_{ex} = 365 nm (using an UV lamp) leads to a blue emission of the colloidal aqueous solutions of CD1 and CD2 (**Figure 2a** and **2b**). This PL originates from the broad absorption bands found in the UV region of both CDs (**Figure 2c** and **2d**). For solutions of CD1 (**Figure 2c**), distinct absorption shoulders at ≤ 250 nm, clear peaks at 355 nm with a narrow full width half maximum (FWHM) of 65 nm as well as shoulders located at 440 nm that extend over the visible spectral range (inset of **Figure 2c**) are obtained. According to literature,[77,78] absorption around 250 nm is assigned to a π-π^* transition of the aromatic C=C bond, and the peak at 355 nm is referred to as n-π^* transition of the C=O bond. The extended absorption band at >440 nm may arise from the complex ligand shell at the CD surface and is sometimes referred to as surface state transition.[77] It is found that this surface-related absorption appears to be an order in magnitude weaker than the n-π^* absorption and can only be monitored at rather high concentrations of CD1, *e.g.* ≥$7.5 \cdot 10^{-3}$ wt%. In the case of CD2 (*cf.* **Figure 2d**), the π-π^* transition shows two peaks located at 255 and 286 nm, which are assigned to C=C and C=N bonds in the aromatic domains, respectively.[79] In comparison to CD1, the major n-π^* transition of CD2 is red-shifted with a peak wavelength of 386 nm (FWHM ≈ 53 nm). The extended shoulder in the range of ~440 to 460 nm (*cf*. inset in **Figure 2d**) indicates the presence of an additional energy level in the electronic structure of CD2. According to literature[80], this shoulder is characteristic for n-π^* transition of C=N bonds which are more abundant in the CD-specific fluorophore of CD2 than in CD1.

Excitation with wavelengths corresponding to the n-π^* transitions of CD1 (λ_{ex} = 355 nm) and CD2 (λ_{ex} = 385 nm) leads to strong PL in the wavelength region of 430–451 nm and 430–436 nm, respectively (**Figure 2e** and **Figure 2f**). Interestingly, increasing the concentration of CD1 from $6.25 \cdot 10^{-4}$ to 10^{-2} wt% progressively shifts the PL emission from 430 nm to 451 nm, whereas the spectral position of the emission of CD2 remain nearly unchanged (430 nm to 436 nm, respectively). This observation is ascribed to concentration-dependent reabsorption (or inner filter) effects (see also **Figure S2a-c**, **SI** section S4) that are more pronounced for CD1 revealing a larger spectral overlap between absorption and emission.[55,77] Moreover, the absorption at ~440 nm is distinctly broader for CD1 than for CD2 (*cf*. inset of **Figure 2c** and **2d**) indicating that photons emitted after excitation at the efficient n-π^* transition of CD1 are likely to be reabsorbed by the surface-state transitions over a wide energy range leading to clearly red-shifted PL emission of CD1 (*cf.* **Figure 2e** and **Figure 2f**). Meng *et al*.[81] also reported PL red-shifts for increasing CD concentrations, which were ascribed to concentration-induced morphological changes and intermolecular interactions affecting the particle surface states and eventually reducing the surface electric potentials of the CDs, favoring CD agglomeration or aggregation. Desorption of surface moieties or adsorbed molecules at lower concentration or upon dilution has been reported to result in concentration-dependent QY values for semiconductor quantum dots.[82,83] However, for the CD systems under investigation this potential explanation seems to be rather unlikely.

For excitation within the wavelength region of the *n*-π^* transition (325 – 385 nm), QY values of 21–40% and 36–48% are obtained for CD1 and CD2, respectively (**Figure 2g** and **2h**). The excitation-dependent QY characteristic is also highlighted by comparison to the respective absorption spectra, where a clear difference between the two systems can be observed. For CD1, the QY profiles match with the absorption spectra in the respective wavelengths range. This is also observed for CD2 for wavelengths >355 nm. However, for wavelengths <355 nm the QY of CD2 drops although the absorption in this wavelength region increases. This demonstrates, that only weak fluorescence originates from the π-π^* transition which is in good agreement to other reports on the PL of CDs.[17,79,84] The fact, that the dissolved precursor materials show different absorption and PL characteristics compared with the corresponding CDs (see SI, **Figure S3, SI** section S5), indicates that the optical properties of the CDs are controlled by the chemical structures of the fluorophores formed during hydrothermal reaction rather than by non-reacted precursors attached to the CD surface.

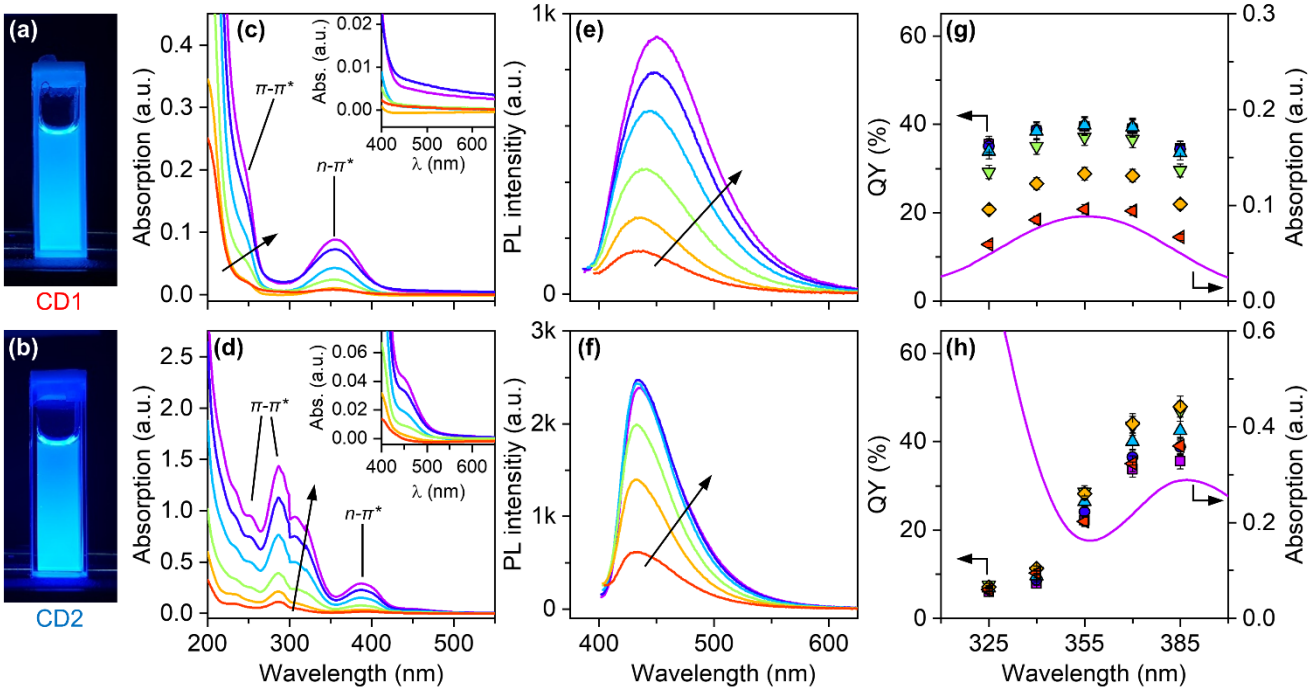

Figure 2. (a, **b)** Photographs of cuvettes filled with aqueous solutions of CD1 (top row) and CD2 (bottom row) excited with UV light; **(c**, **d)** Absorption spectra of CD solutions with concentrations of $6.25\cdot10^{-4}$, $1.25\cdot10^{-3}$, $2.5\cdot10^{-3}$, $5\cdot10^{-3}$, $7.5\cdot10^{-3}$ and 10^{-2} wt% (increasing concentration indicated by arrows); **(e**, **f)** PL with excitation wavelength at the *n*-π^* energy ($\lambda_{ex,CD1}$ = 355 nm and $\lambda_{ex,CD2}$ = 385 nm) resulting in a blue emission at 430–451 nm and 430–436 nm for CD1 and CD2, respectively. **(g**, **h)** Absolute quantum yields [symbols: triangle pointing left ($6.25\cdot10^{-4}$ wt%), diamond ($1.25\cdot10^{-3}$ wt%), triangle pointing downwards ($2.5\cdot10^{-3}$ wt%), triangle pointing upwards ($5\cdot10^{-3}$ wt%), circle ($7.5\cdot10^{-3}$ wt%) and square (10^{-2} wt%)] of CD1 and CD2 are at 21–40% and 36–48% for photoexcitation at 325, 340, 355, 370 and 385 nm. A comparison to the absorption spectra (lines, obtained with 10^{-2} wt% CD solutions) suggests that the high QY is solely obtained for excitation at the *n*-π^* transition.

3.3. pH-dependent optical properties of CDs. In aqueous dispersions, the polar functional groups of CD1 and CD2 interact with water molecules (forming a protective shell at the CD surface) and the pH of

the solution can affect the protonation state of the surface groups and surface-bound fluorophores resulting in pH-dependent optical properties as revealed by acid-base titrations (*cf*. **SI**, section S1 for details). The photographs in **Figure 3a** and **3b** clearly show a different PL emission behavior of CD1 and CD2 attributed to the change in pH value. The CD concentration in each sample remained constant at $5 \cdot 10^{-3}$ wt%. Absorption spectra in the pH range 1–12 reveal that the positions of the *n*-π^* transition in CD1 and CD2 change with pH (**Figure 3c** and **3d**). Additionally, also the spectral positions of the PL bands shift (**Figure 3e** and **3f**) confirming that the energy levels and electronic transitions in CD1 and CD2 which are involved in radiative recombination processes depend on the pH of the solvent. These pH-induced spectral changes in peak position and intensity are almost completely reversible indicating almost negligible pH-induced degradation of CDs or dissociation of the surface groups/fluorophores (**Figure 3g**, **3f,** and **3h** and **SI**, section S6, **Figure S4**).

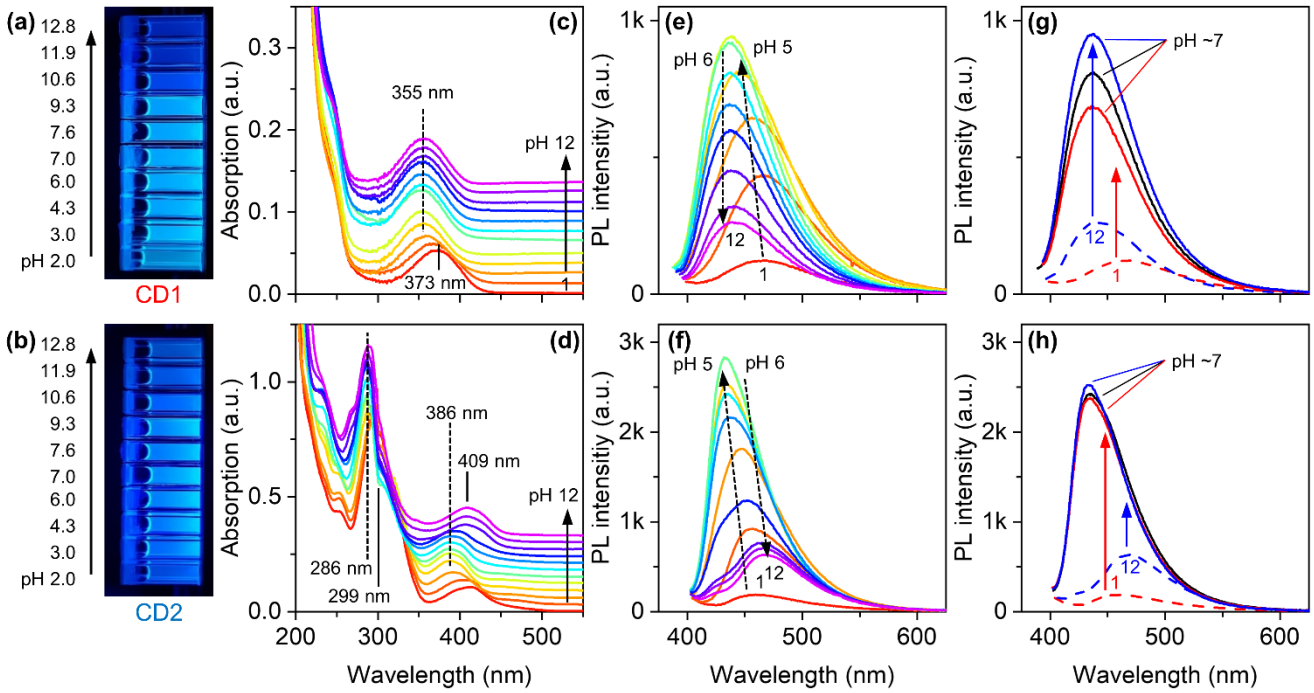

Figure 3. (a, **b)** Photographs of CD1 (top row) and CD2 (bottom row) solutions in aqueous solution for different pH. Excitation with UV light reveals pH-dependent changes of the blue emission for both CDs; **(c**, **d)** Increasing the pH from 1 (red) to 12 (purple) results in wavelength shifts of the absorption spectra, particularly in the region of the *n*-π^* transition, relative to the absorption bands obtained at pH 7 (dashed line); **(e**, **f)** The PL peak emission shifts towards longer wavelength under strong acidic conditions for CD1, while in the case of CD2 both low and high pH values result in a red-shifted emission; **(g**, **h)** Reversing the pH from 1 or 12 (dashed lines) to neutral conditions (pH ~7) shows a nearly complete recovery suggesting negligible pH-induced degradation. The CD concentration was always kept constant at $5 \cdot 10^{-3}$ wt%.

Figure 4a shows the pH-dependence of the absorption peak wavelength of the *n*-π^* transitions for pH values of 1–12. In the case of pH < 4, bathochromic shifts are obtained for both CD1 and CD2, resulting in peaks at 373 and 412 nm for pH ~1, respectively. Interestingly, for high pH conditions, bathochromic shifts are solely obtained in the case of CD2 (absorption maximum at 409 nm at pH ~12), while the

spectral position of the *n*-π^* electron transition of CD1 remains unaffected in the pH range 4–12. The latter is in excellent agreement to previously reported carbon dots synthesized from citric acid and monomeric ethylenediamine.[76] The PL peak wavelengths of both CDs reveal comparable pH-dependent characteristics (**Figure 4b**). The emission wavelength of CD1 excited at 355 nm shifts from 438 nm (pH ~7) to 467 nm (pH ~1) and remains constant for high pH values, while CD2 (excited at 385 nm) exhibits shifts of the PL wavelength from 436 nm (pH ~7) to 460 (pH ~1) and 467 nm (pH ~12), respectively. The pH-dependent characteristics of the PL FWHM (**Figure 4c**) of CD1 and CD2 follows a similar trend as the absorption and emission peaks, revealing a spectral broadening at acidic pH (CD1: FWHM ~75 nm for pH > 4 and ~92 nm for pH ~1; CD2: FWHM ~53 nm for pH ~5 and ~76 and 77 nm at pH values of ~1 and ~10, respectively). In both systems, the highest QY values of 50.6 and 55.6 % are obtained at pH ~5 and ~6 for CD1 and CD2, respectively (**Figure 4d**). The QY values decrease at lower and higher pH values indicating the importance of the protonation state of the surface groups and surface-bound fluorophores for optimum QY. In addition, the pH-dependency of the electrical mobilities of CD1 and CD2 were measured (**Figure 4e**) in order to derive the corresponding zeta potentials (**Figure 4f**). In colloidal chemistry, as a rule of thumb, sufficient colloidal stability of particle dispersions is obtained below -30 mV (or above +30 mV) due to the electrostatic repulsion of the particles.[40,85] This criterion is fulfilled for pH 5–12 and 5–11 for CD1 and CD2, respectively. The resulting increase in zeta potential of CD2 at pH >11 presumably originates from a compression of the double layer.[40] The pH-dependent zeta potential profiles observed for CD1 and CD2, that resemble those previously reported for graphene nanosheets,[85] are ascribed to the (de-)protonation of pH active surface groups and functionalities in the surface bound fluorophores.

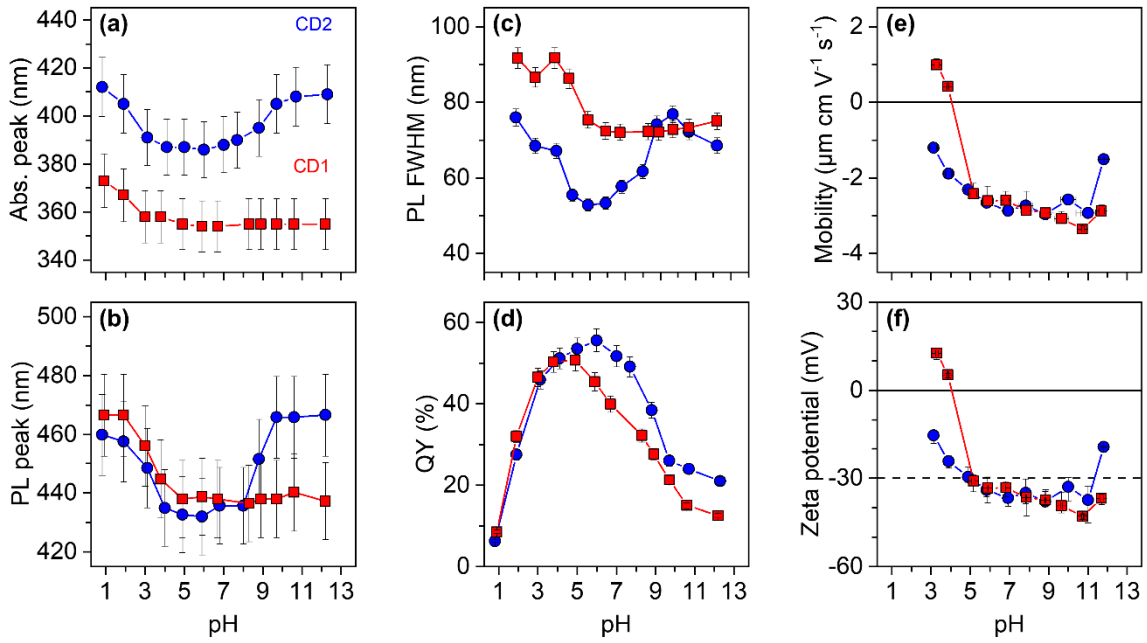

Figure 4. pH-Induced changes of **(a)** the intensity of the *n*-π^* transition, **(b)** the PL peak wavelength, **(c)** the FWHM of the PL band, **(d)** the QY, **(e)** the mobility, and **(f)** the Zeta potential (ZP) of CD1 (red squares) and CD2 (blue circles), respectively. The PL of CD1 and CD2 ($5 \cdot 10^{-3}$ wt%) were excited at 355 nm and 385 nm. At pH <4, bathochromic shifts of the absorption and PL bands are observed for both CD samples. At pH >8, bathochromic absorption and emission shifts solely occur for CD2, while CD1

shows no significant changes in the pH range 4–12. QY show a similar pH-dependency for both CD samples with maximal values of >40% for pH 4–8. **(e**, **f)** Mobilities were measured and applied for calculation of the zeta potentials of the CDs.

In **Scheme 2**, the observed pH-dependencies are associated with the pK_a values of the pH active functional groups present on the CD surface and in the surface-bound fluorophores. The pKa values of the carboxylic groups ($pK_a \approx 4–5$),[17,40] and the pyridine nitrogen ($pK_a \approx 4–6$)[86] are lower than those of primary amine (NH_2) groups ($pK_a \approx 9–11$)[86] or phenolic OH groups ($pK_a \approx 8–10$)[17,86] as well as amide C(=O)(-NH) groups ($pK_a \approx >8.5$)[86]. This suggests that the protonation of carboxylic and/or pyridine nitrogen moieties is responsible for the observed red-shifts of the absorption and emission peaks of CD1 and CD2 at low pH (*cf*. **Figure 4a**, **4b**). This presumption also agrees with the observation of positive zeta potentials in CD1 which are assumed to result from protonating carboxylate (COO^-) groups to carboxyl groups (COOH) for pH < ~4.[17,40] Moreover, amides and fluorophore moieties in CD1 and CD2 possess carboxylates as residues from the reaction between CA and the amine precursor, which could directly affect the *n*-*π** electron transitions upon protonation at low pH and therefore trigger the observed red-shifts. The much stronger response of the optical properties of CD2 to basic pH values are attributed to a more pronounced influence of the phenolic OH, amides and/or amines on the optical characteristics of CD2. Formation of phenolate anions ($Ar\text{-}O^-$) at high pH could lead to more non-bonding and delocalized electrons explaining the bathochromic shifts obtained in CD2.[17] The absence of bathochromic shifts for CD1 at high pH conditions is ascribed to the fact that residual amine moieties from the PEI molecule occupy a major fraction of the CD surface. Therefore, an enhanced deprotonation of the accessible amine groups ($-NH_3^+ \rightarrow -NH_2$) in CD1 at high pH is conceivable without affecting the *n*-*π** energy levels. Apparently, also the *π*-*π** transitions attributed to the graphitic core of CD1 are less pH-responsive than those found for CD2 (*cf*. **Figure 3c**, **3d**). This strengthens the hypothesis that extended amine moieties at the surface of CD1 sufficiently stabilize and shield the particles at basic conditions, whereas the shorter surface moieties and fluorophores of CD2 provide less stabilization and protection allowing pH-induced energy shifts for the *n*-*π** and *π*-*π** transitions.

The observed spectral broadening of the absorption bands of CD1 and CD2 (*cf*. **Figure 4c**) might be attributed to hydrogen bonding interactions between carboxyl and phenol groups at the surface with the sp^2 carbon core domains[17] and vibrational coupling effects based on intra (within the carbon dots) and inter (between CD and water) hydrogen-bonds. We tentatively ascribe the broader emission peak observed for CD1 (larger FWHM) upon protonation of the carboxylate groups at low pH and the deprotonation of phenol at high pH to changes in the number of hydrogen bonds.

The reduction of QY at extreme acidic or basic pH conditions could result from enhanced non-radiative processes (*cf*. **Figure 4d**) as a consequence of the selective (de-)protonation of surface functionalities. Interestingly, even if the QYs of both CDs decrease at high pH conditions, it is remarkable that the *n*-*π** transition energies of CD1 remain rather unaffected. These findings suggest that the different pH-dependent optical properties of CD1 and CD2 result from the different amine precursors used during their synthesis.

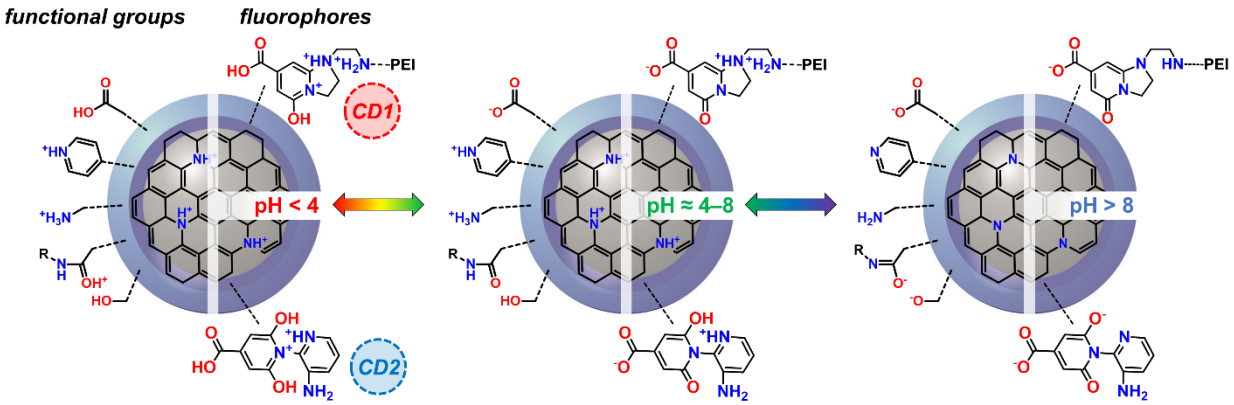

Scheme 2. pH-dependent changes of CD1 and CD2 attributed to the (de-)protonation of the different functional surface groups and fluorophores. The amine precursors, PEI and DAP, provide different molecular structures that are supposed to impact the rest "R" in the surface amides. Here, PEI features abundant NH_2 groups and a long polymer chain that might compensate alkaline solvent conditions without disturbing the energy bands of the CDs.

4. Conclusion and Outlook

In conclusion, we could demonstrate that the type of amine precursor used during the hydrothermal synthesis of carbon dots (CDs) with citric acid directly affects the absorption and emission features of the resulting nanomaterial and can be exploited for tuning of the optical properties. By employing an amine precursor such as 2,3-diaminopyridine (DAP) which possess aromatic nitrogen groups increases the amount of sp^2-hybridized nitrogen atoms in the products. Therefore, the fluorescent moieties governing the emission of CD2 possess an expanded conjugation revealed by a *n*-π^* absorption band which is red-shifted relative to that observed for CD1. Moreover, excitation of CD1 and CD2 with photons of energies matching the respective *n*-π^* transitions resulted in an efficient light emission with high quantum yields (QYs) of ~40% and ~48%, respectively. This is a relevant finding for the design of optoelectronic devices based on these environmentally friendly and easily accessible organic materials.[87] The use of CDs as converter material for inorganic light emitting diodes (LEDs) would also involve the functionalization of the semiconductor surface (*e.g.* gallium nitride), and the interaction of the CD materials with the solid crystal, in particular its charged surface states including the respective field effects, should be understood and adjusted to obtain an optimum luminescence efficiency.

Moreover, we investigated the pH-dependence of the optical properties of CD1 and CD2. Our results show comparable shifts of the *n*-π^* absorption bands at pH < 8 attributed to protonation of carboxylic groups and/or pyridine nitrogen atoms. In contrast, in the pH range of 8–12 solely the *n*-π^* absorption band of CD2 underwent a red-shift. In the case of CD1 the *n*-π^* transition remained nearly pH-independent which could originate from the large amount of amine moieties from polyethylenimine (PEI) precursor present in this CD in comparison to DAP used for the preparation of CD2. Hence, at basic conditions, mainly the abundantly present amine groups from the polymer deprotonated. The sequence of (de-)protonation of the surface groups and surface bound fluorophores of the CDs could be possibly exploited for pH sensing.

Acknowledgements

This work was realized with the financial support by the DFG FOR 1616 Dynamics and Interactions of Semiconductor Nano- wires for Optoelectronics". F.M. and T.V. also acknowledge the financial support by the "Niedersächsisches Vorab" and the "Quantum- and Nano-Metrology (QUANOMET)" initiative within the project NP-3 "Modell-Nanopartikel". K.M.-C. acknowledges funding from the Initiative and Network Fund of the Helmholtz Association under Contract No. NG-1317. F.W. and U.R.-G. gratefully acknowledge the financial support from the German Research Council (DFG; RE1203/12-3). F.D. and S.R.W. are thankful for the financial support by DFG, WA1276/7-2.

Supporting Information descriptions

Section S1: Detailed experimental methods for CD synthesis and preparation of CD solutions; Section S2: Additional details of FTIR analysis for precursors and CDs; Section S3: Mass spectra of CDs; Section S4: Concentration-dependent properties of CDs; Section S5: Optical properties of precursors (CA, PEI and DAP); Section S6: Reversibility of pH-dependent optical properties; Section S7: Optical properties of CD1 (crude) and CD2 (Cl).

References

(1) Xu, X.; Ray, R.; Gu, Y.; Ploehn, H. J.; Gearheart, L.; Raker, K.; Scrivens, W. A. Electrophoretic Analysis and Purification of Fluorescent Sing-Walled Carbon Nanotube Fragments. *Journal of the American Chemical Society* **2004**, *126*, 12736–12737.

(2) Sun, Y. P.; Zhou, B.; Lin, Y.; Wang, W.; Fernando, K. A. S.; Pathak, P.; Meziani, M. J.; Harruff, B. A.; Wang, X.; Wang, H.; et al. Quantum-Sized Carbon Dots for Bright and Colorful Photoluminescence. *Journal of the American Chemical Society* **2006**, *128* (24), 7756–7757.

(3) Zheng, L.; Chi, Y.; Dong, Y.; Lin, J.; Wang, B. Electrochemiluminescence of Water-Soluble Carbon Nanocrystals Released Electrochemically from Graphite. *Journal of the American Chemical Society* **2009**, *131* (13), 4564–4565.

(4) Wang, F.; Chen, Y. H.; Liu, C. Y.; Ma, D. G. White Light-Emitting Devices Based on Carbon Dots' Electroluminescence. *Chemical Communications* **2011**, *47* (12), 3502–3504.

(5) Zhang, X.; Zhang, Y.; Wang, Y.; Kalytchuk, S.; Kershaw, S. V; Wang, Y.; Wang, P.; Zhang, T.; Zhao, Y.; Zhang, H.; et al. Color-Switchable Electroluminescence of Carbon Dot Light-Emitting Diodes. *ACS Nano* **2013**, *7* (12), 11234–11241.

(6) Yuan, F.; Wang, Z.; Li, X.; Li, Y.; Tan, Z.; Fan, L.; Yang, S. Bright Multicolor Bandgap Fluorescent Carbon Quantum Dots for Electroluminescent Light-Emitting Diodes. *Advanced Materials* **2017**, *29* (3), 1604436.

(7) Yuan, F.; Yuan, T.; Sui, L.; Wang, Z.; Xi, Z.; Li, Y.; Li, X.; Fan, L.; Tan, Z.; Chen, A.; et al. Engineering Triangular Carbon Quantum Dots with Unprecedented Narrow Bandwidth Emission for Multicolored LEDs. *Nature Communications* **2018**, *9* (1), 2249.

(8) Baker, S. N.; Baker, G. A. Luminescent Carbon Nanodots: Emergent Nanolights. *Angewandte Chemie - International Edition* **2010**, *49* (38), 6726–6744.

(9) Li, H.; Kang, Z.; Liu, Y.; Lee, S. T. Carbon Nanodots: Synthesis, Properties and Applications. *Journal of Materials Chemistry* **2012**, *22* (46), 24230–24253.

(10) Park, Y.; Yoo, J.; Lim, B.; Kwon, W.; Rhee, S. W. Improving the Functionality of Carbon Nanodots: Doping and Surface Functionalization. *Journal of Materials Chemistry A* **2016**, *4* (30), 11582–11603.

(11) Reckmeier, C. J.; Wang, Y.; Zboril, R.; Rogach, A. L. Influence of Doping and Temperature on Solvatochromic Shifts in Optical Spectra of Carbon Dots. *Journal of Physical Chemistry C* **2016**, *120* (19), 10591–10604.

(12) Yang, Z.; Li, Z.; Xu, M.; Ma, Y.; Zhang, J.; Su, Y.; Gao, F.; Wei, H.; Zhang, L. Controllable Synthesis of Fluorescent Carbon Dots and Their Detection Application as Nanoprobes. *Nano-Micro Letters* **2013**, *5* (4), 247–259.

(13) Gao, F.; Ma, S.; Li, J.; Dai, K.; Xiao, X.; Zhao, D.; Gong, W. Rational Design of High Quality Citric Acid-Derived Carbon Dots by Selecting Efficient Chemical Structure Motifs. *Carbon* **2017**, *112*, 131–141.

(14) Dissinger, F.; Zimmermann, K.; Jaros, A.; Meierhofer, F.; Cammi, D.; Voss, T.; Waldvogel, S. R. Red-Shifted Absorption of C-Dots for Utilization in Hybrid Nano-Optoelectronics by Application of Systematically Synthesized Precursor Molecules. *physica status solidi (b)* **2019**, *256* (4), 1800493.

(15) Feng, T.; Zeng, Q.; Lu, S.; Yan, X.; Liu, J.; Tao, S.; Yang, M.; Yang, B. Color-Tunable Carbon Dots Possessing Solid-State Emission for Full-Color Light-Emitting Diodes Applications. *ACS Photonics* **2018**, *5* (2), 502–510.

(16) Konkena, B.; Vasudevan, S. Spectral Migration of Fluorescence in Graphene Oxide Aqueous Dispersions: Evidence for Excited-State Proton Transfer. *The Journal of Physical Chemistry Letters* **2014**, *5* (1), 1–7.

(17) Dutta Choudhury, S.; Chethodil, J. M.; Gharat, P. M.; Praseetha, P. K.; Pal, H. PH-Elicited Luminescence Functionalities of Carbon Dots: Mechanistic Insights. *Journal of Physical Chemistry Letters* **2017**, *8* (7), 1389–1395.

(18) Ehrat, F.; Bhattacharyya, S.; Schneider, J.; Löf, A.; Wyrwich, R.; Rogach, A. L.; Stolarczyk, J. K.; Urban, A. S.; Feldmann, J. Tracking the Source of Carbon Dot Photoluminescence: Aromatic Domains versus Molecular Fluorophores. *Nano Letters* **2017**, *17* (12), 7710–7716.

(19) Essner, J. B.; Kist, J. A.; Polo-Parada, L.; Baker, G. A. Artifacts and Errors Associated with the Ubiquitous Presence of Fluorescent Impurities in Carbon Nanodots. *Chemistry of Materials* **2018**, *30* (6), 1878–1887.

(20) Yang, Y.; Cui, J.; Zheng, M.; Hu, C.; Tan, S.; Xiao, Y.; Yang, Q.; Liu, Y. One-Step Synthesis of Amino-Functionalized Fluorescent Carbon Nanoparticles by Hydrothermal Carbonization of Chitosan. *Chemical Communications* **2012**, *48* (3), 380–382.

(21) Krysmann, M. J.; Kelarakis, A.; Dallas, P.; Giannelis, E. P. Formation Mechanism of Carbogenic Nanoparticles with

Dual Photoluminescence Emission. *Journal of the American Chemical Society* **2012**, *134* (2), 747–750.
(22) Dong, Y.; Wang, R.; Li, H.; Shao, J.; Chi, Y.; Lin, X.; Chen, G. Polyamine-Functionalized Carbon Quantum Dots for Chemical Sensing. *Carbon* **2012**, *50* (8), 2810–2815.
(23) Qian, Z.; Ma, J.; Shan, X.; Feng, H.; Shao, L.; Chen, J. Highly Luminescent N-Doped Carbon Quantum Dots as an Effective Multifunctional Fluorescence Sensing Platform. *Chemistry – A European Journal* **2014**, *20* (8), 2254–2263.
(24) Righetto, M.; Privitera, A.; Fortunati, I.; Mosconi, D.; Zerbetto, M.; Curri, M. L.; Corricelli, M.; Moretto, A.; Agnoli, S.; Franco, L.; et al. Spectroscopic Insights into Carbon Dot Systems. *The Journal of Physical Chemistry Letters* **2017**, *8* (10), 2236–2242.
(25) Gan, Z.; Xu, H.; Hao, Y. Mechanism for Excitation-Dependent Photoluminescence from Graphene Quantum Dots and Other Graphene Oxide Derivates: Consensus, Debates and Challenges. *Nanoscale* **2016**, *8* (15), 7794–7807.
(26) Dhenadhayalan, N.; Lin, K.-C.; Suresh, R.; Ramamurthy, P. Unravelling the Multiple Emissive States in Citric-Acid-Derived Carbon Dots. *The Journal of Physical Chemistry C* **2016**, *120* (2), 1252–1261.
(27) Strauss, V.; Margraf, J. T.; Dolle, C.; Butz, B.; Nacken, T. J.; Walter, J.; Bauer, W.; Peukert, W.; Spiecker, E.; Clark, T.; et al. Carbon Nanodots: Toward a Comprehensive Understanding of Their Photoluminescence. *Journal of the American Chemical Society* **2014**, *136* (49), 17308–17316.
(28) Demchenko, A. P.; Dekaliuk, M. O. The Origin of Emissive States of Carbon Nanoparticles Derived from Ensemble-Averaged and Single-Molecular Studies. *Nanoscale* **2016**, *8* (29), 14057–14069.
(29) Reckmeier, C. J.; Schneider, J.; Xiong, Y.; Häusler, J.; Kasák, P.; Schnick, W.; Rogach, A. L. Aggregated Molecular Fluorophores in the Ammonothermal Synthesis of Carbon Dots. *Chemistry of Materials* **2017**, *29* (24), 10352–10361.
(30) Wang, L.; Zhu, S. J.; Wang, H. Y.; Qu, S. N.; Zhang, Y. L.; Zhang, J. H.; Chen, Q. D.; Xu, H. L.; Han, W.; Yang, B.; et al. Common Origin of Green Luminescence in Carbon Nanodots and Graphene Quantum Dots. *ACS Nano* **2014**, *8* (3), 2541–2547.
(31) Khan, S.; Gupta, A.; Verma, N. C.; Nandi, C. K. Time-Resolved Emission Reveals Ensemble of Emissive States as the Origin of Multicolor Fluorescence in Carbon Dots. *Nano Letters* **2015**, *15* (12), 8300–8305.
(32) Sharma, A.; Gadly, T.; Gupta, A.; Ballal, A.; Ghosh, S. K.; Kumbhakar, M. Origin of Excitation Dependent Fluorescence in Carbon Nanodots. *Journal of Physical Chemistry Letters* **2016**, *7* (18), 3695–3702.
(33) Kumar, P.; Bohidar, H. B. Observation of Fluorescence from Non-Functionalized Carbon Nanoparticles and Its Solvent Dependent Spectroscopy. *Journal of Luminescence* **2013**, *141*, 155–161.
(34) Hola, K.; Bourlinos, A. B.; Kozak, O.; Berka, K.; Siskova, K. M.; Havrdova, M.; Tucek, J.; Safarova, K.; Otyepka, M.; Giannelis, E. P.; et al. Photoluminescence Effects of Graphitic Core Size and Surface Functional Groups in Carbon Dots: COO− Induced Red-Shift Emission. *Carbon* **2014**, *70*, 279–286.
(35) Sciortino, A.; Marino, E.; Dam, B. van; Schall, P.; Cannas, M.; Messina, F. Solvatochromism Unravels the Emission Mechanism of Carbon Nanodots. *The Journal of Physical Chemistry Letters* **2016**, *7* (17), 3419–3423.
(36) Liu, H.; Ye, T.; Mao, C. Fluorescent Carbon Nanoparticles Derived from Candle Soot. *Angewandte Chemie International Edition* **2007**, *46* (34), 6473–6475.
(37) Pan, D.; Zhang, J.; Li, Z.; Wu, M. Hydrothermal Route for Cutting Graphene Sheets into Blue-Luminescent Graphene Quantum Dots. *Advanced Materials* **2010**, *22* (6), 734–738.
(38) Chen, J.-L.; Yan, X.-P. Ionic Strength and PH Reversible Response of Visible and Near-Infrared Fluorescence of Graphene Oxide Nanosheets for Monitoring the Extracellular PH. *Chemical Communications* **2011**, *47* (11), 3135–3137.
(39) Zhu, S.; Zhang, J.; Qiao, C.; Tang, S.; Li, Y.; Yuan, W.; Li, B.; Tian, L.; Liu, F.; Hu, R.; et al. Strongly Green-Photoluminescent Graphene Quantum Dots for Bioimaging Applications. *Chemical Communications* **2011**, *47* (24), 6858–6860.
(40) Konkena, B.; Vasudevan, S. Understanding Aqueous Dispersibility of Graphene Oxide and Reduced Graphene Oxide through PKa Measurements. *The Journal of Physical Chemistry Letters* **2012**, *3* (7), 867–872.
(41) Ye, R.; Xiang, C.; Lin, J.; Peng, Z.; Huang, K.; Yan, Z.; Cook, N. P.; Samuel, E. L. G.; Hwang, C.-C.; Ruan, G.; et al. Coal as an Abundant Source of Graphene Quantum Dots. *Nature Communications* **2013**, *4*, 2943.
(42) Kozawa, D.; Miyauchi, Y.; Mouri, S.; Matsuda, K. Exploring the Origin of Blue and Ultraviolet Fluorescence in Graphene Oxide. *The Journal of Physical Chemistry Letters* **2013**, *4* (12), 2035–2040.
(43) Hu, L.; Sun, Y.; Li, S.; Wang, X.; Hu, K.; Wang, L.; Liang, X.; Wu, Y. Multifunctional Carbon Dots with High Quantum Yield for Imaging and Gene Delivery. *Carbon* **2014**, *67*, 508–513.
(44) Jia, X.; Yang, X.; Li, J.; Li, D.; Wang, E. Stable Cu Nanoclusters: From an Aggregation-Induced Emission Mechanism to Biosensing and Catalytic Applications. *Chemical Communications* **2014**, *50* (2), 237–239.
(45) Kong, W.; Wu, H.; Ye, Z.; Li, R.; Xu, T.; Zhang, B. Optical Properties of PH-Sensitive Carbon-Dots with Different Modifications. *Journal of Luminescence* **2014**, *148*, 238–242.
(46) Sachdev, A.; Matai, I.; Gopinath, P. Implications of Surface Passivation on Physicochemical and Bioimaging Properties of Carbon Dots. *RSC Advances* **2014**, *4* (40), 20915–20921.
(47) Song, Y.; Zhu, S.; Xiang, S.; Zhao, X.; Zhang, J.; Zhang, H.; Fu, Y.; Yang, B. Investigation into the Fluorescence Quenching Behaviors and Applications of Carbon Dots. *Nanoscale* **2014**, *6* (9), 4676–4682.
(48) Wu, Z. L.; Gao, M. X.; Wang, T. T.; Wan, X. Y.; Zheng, L. L.; Huang, C. Z. A General Quantitative PH Sensor Developed with Dicyandiamide N-Doped High Quantum Yield Graphene Quantum Dots. *Nanoscale* **2014**, *6* (7), 3868–3874.
(49) Yuan, F.; Ding, L.; Li, Y.; Li, X.; Fan, L.; Zhou, S.; Fang, D.; Yang, S. Multicolor Fluorescent Graphene Quantum Dots Colorimetrically Responsive to All-PH and a Wide Temperature Range. *Nanoscale* **2015**, *7* (27), 11727–11733.
(50) Wang, C.; Xu, Z.; Zhang, C. Polyethyleneimine-Functionalized Fluorescent Carbon Dots: Water Stability, PH Sensing, and Cellular Imaging. *ChemNanoMat* **2015**, *1* (2), 122–127.
(51) Wang, C.; Xu, Z.; Cheng, H.; Lin, H.; Humphrey, M. G.; Zhang, C. A Hydrothermal Route to Water-Stable Luminescent Carbon Dots as Nanosensors for PH and Temperature. *Carbon* **2015**, *82*, 87–95.
(52) Zheng, C.; An, X.; Gong, J. Novel PH Sensitive N-Doped Carbon Dots with Both Long Fluorescence Lifetime and High Quantum Yield. *RSC Advances* **2015**, *5* (41), 32319–32322.
(53) Pan, D.; Zhang, J.; Li, Z.; Wu, C.; Yan, X.; Wu, M. Observation of PH-, Solvent-, Spin-, and Excitation-Dependent Blue Photoluminescence from Carbon Nanoparticles. *Chemical Communications* **2010**, *46* (21), 3681–3683.
(54) Qiao, Z.-A.; Wang, Y.; Gao, Y.; Li, H.; Dai, T.; Liu, Y.; Huo, Q. Commercially Activated Carbon as the Source for Producing Multicolor Photoluminescent Carbon Dots by Chemical Oxidation. *Chemical Communications* **2010**, *46* (46), 8812–8814.
(55) Dong, Y.; Wang, R.; Li, G.; Chen, C.; Chi, Y.; Chen, G. Polyamine-Functionalized Carbon Quantum Dots as Fluorescent Probes for Selective and Sensitive Detection of Copper Ions. *Anal. Chem.* **2012**, *84* (14), 6220–6224.

(56) Jia, X.; Li, J.; Wang, E. One-Pot Green Synthesis of Optically PH-Sensitive Carbon Dots with Upconversion Luminescence. *Nanoscale* **2012**, *4* (18), 5572–5575.
(57) Liu, C.; Zhang, P.; Zhai, X.; Tian, F.; Li, W.; Yang, J.; Liu, Y.; Wang, H.; Wang, W.; Liu, W. Nano-Carrier for Gene Delivery and Bioimaging Based on Carbon Dots with PEI-Passivation Enhanced Fluorescence. *Biomaterials* **2012**, *33* (13), 3604–3613.
(58) Shi, W.; Li, X.; Ma, H. A Tunable Ratiometric PH Sensor Based on Carbon Nanodots for the Quantitative Measurement of the Intracellular PH of Whole Cells. *Angewandte Chemie International Edition* **2012**, *51* (26), 6432–6435.
(59) Guo, Y.; Wang, Z.; Shao, H.; Jiang, X. Hydrothermal Synthesis of Highly Fluorescent Carbon Nanoparticles from Sodium Citrate and Their Use for the Detection of Mercury Ions. *Carbon* **2013**, *52*, 583–589.
(60) Shen, L.; Zhang, L.; Chen, M.; Chen, X.; Wang, J. The Production of PH-Sensitive Photoluminescent Carbon Nanoparticles by the Carbonization of Polyethylenimine and Their Use for Bioimaging. *Carbon* **2013**, *55*, 343–349.
(61) Hu, S.; Trinchi, A.; Atkin, P.; Cole, I. Tunable Photoluminescence across the Entire Visible Spectrum from Carbon Dots Excited by White Light. *Angewandte Chemie - International Edition* **2015**, *54* (10), 2970–2974.
(62) Cammi, D.; Zimmermann, K.; Gorny, R.; Vogt, A.; Dissinger, F.; Gad, A.; Markiewcz, N.; Waag, A.; Prades, J. D.; Ronning, C.; et al. Enhancement of the Sub-Band-Gap Photoconductivity in ZnO Nanowires through Surface Functionalization with Carbon Nanodots. *The Journal of Physical Chemistry C* **2018**, *122* (3), 1852–1859.
(63) Zimmermann, K.; Dissinger, F.; Cammi, D.; Jaros, A.; Meierhofer, F.; Waldvogel, S. R.; Voss, T. Shifting the Photoresponse of ZnO Nanowires into the Visible Spectral Range by Surface Functionalization with Tailor-Made Carbon Nanodots. *The Journal of Physical Chemistry C* **2018**, *122* (51), 29479–29487.
(64) Song, Y.; Zhu, S.; Zhang, S.; Fu, Y.; Wang, L.; Zhao, X.; Yang, B. Investigation from Chemical Structure to Photoluminescent Mechanism: A Type of Carbon Dots from the Pyrolysis of Citric Acid and an Amine. *Journal of Materials Chemistry C* **2015**, *3* (23), 5976–5984.
(65) Kasprzyk, W.; Bednarz, S.; Zmudzki, P.; Galica, M.; Bogdał, D. Novel Efficient Fluorophores Synthesized from Citric Acid. *RSC Advances* **2015**, *5* (44), 34795–34799.
(66) Schneider, J.; Reckmeier, C. J.; Xiong, Y.; Von Seckendorff, M.; Susha, A. S.; Kasak, P.; Rogach, A. L. Molecular Fluorescence in Citric Acid-Based Carbon Dots. *Journal of Physical Chemistry C* **2017**, *121* (3), 2014–2022.
(67) Bhattacharyya, S.; Ehrat, F.; Urban, P.; Teves, R.; Wyrwich, R.; Döblinger, M.; Feldmann, J.; Urban, A. S.; Stolarczyk, J. K. Effect of Nitrogen Atom Positioning on the Trade-off between Emissive and Photocatalytic Properties of Carbon Dots. *Nature Communications* **2017**, *8* (1), 1401.
(68) Tehan, B. G.; Lloyd, E. J.; Wong, M. G.; Pitt, W. R.; Montana, J. G.; Manallack, D. T.; Gancia, E. Estimation of PKa Using Semiempirical Molecular Orbital Methods. Part 1: Application to Phenols and Carboxylic Acids. *Quantitative Structure-Activity Relationships* **2002**, *21* (5), 457–472.
(69) Tehan, B. G.; Lloyd, E. J.; Wong, M. G.; Pitt, W. R.; Gancia, E.; Manallack, D. T. Estimation of PKa Using Semiempirical Molecular Orbital Methods. Part 2: Application to Amines, Anilines and Various Nitrogen Containing Heterocyclic Compounds. *Quantitative Structure-Activity Relationships* **2002**, *21* (5), 473–485.
(70) Würth, C.; Grabolle, M.; Pauli, J.; Spieles, M.; Resch-Genger, U. Relative and Absolute Determination of Fluorescence Quantum Yields of Transparent Samples. *Nature Protocols* **2013**, *8*, 1535–1550.
(71) Oomens, J.; Steill, J. D. Free Carboxylate Stretching Modes. *The Journal of Physical Chemistry A* **2008**, *112* (15), 3281–3283.
(72) Parker, F.; Kirschenbaum, D. An Infrared Spectrophotmetric Study of the Phenol-Phenoxide Dissociation. *The Journal of Physical Chemistry* **1959**, *63* (8), 1342–1344.
(73) Koleva, B. B.; Kolev, T.; Tsanev, T.; Kotov, S.; Mayer-Figge, H.; Seidel, R. W.; Sheldrick, W. S. Spectroscopic and Structural Elucidation of 3,4-Diaminopyridine and Its Hydrogentartarate Salt: Crystal Structure of 3,4-Diaminopyridinium Hydrogentartarate Dihydrate. *Journal of Molecular Structure* **2008**, *881* (1–3), 146–155.
(74) Szabó, T.; Berkesi, O.; Forgó, P.; Josepovits, K.; Sanakis, Y.; Petridis, D.; Dékány, I. Evolution of Surface Functional Groups in a Series of Progressively Oxidized Graphite Oxides. *Chemistry of Materials* **2006**, *18* (11), 2740–2749.
(75) Reckmeier, C. J.; Schneider, J.; Xiong, Y.; Häusler, J.; Kasák, P.; Schnick, W.; Rogach, A. L. Aggregated Molecular Fluorophores in the Ammonothermal Synthesis of Carbon Dots. *Chemistry of Materials* **2017**, *29* (24), 10352–10361.
(76) Stepanidenko, E. A.; Arefina, I. A.; Khavlyuk, P. D.; Dubavik, A.; Bogdanov, K. V; Bondarenko, D. P.; Cherevkov, S. A.; Kundelev, E. V; Fedorov, A. V; Baranov, A. V; et al. Influence of the Solvent Environment on Luminescent Centers within Carbon Dots. *Nanoscale* **2020**, *12* (2), 602–609.
(77) Wang, Y.; Kalytchuk, S.; Zhang, Y.; Shi, H.; Kershaw, S. V.; Rogach, A. L. Thickness-Dependent Full-Color Emission Tunability in a Flexible Carbon Dot Ionogel. *Journal of Physical Chemistry Letters* **2014**, *5* (8), 1412–1420.
(78) Luo, Z.; Lu, Y.; Somers, L. A.; Johnson, A. T. C. High Yield Preparation of Macroscopic Graphene Oxide Membranes. *Journal of the American Chemical Society* **2009**, *131* (3), 898–899.
(79) Ding, H.; Yu, S. B.; Wei, J. S.; Xiong, H. M. Full-Color Light-Emitting Carbon Dots with a Surface-State-Controlled Luminescence Mechanism. *ACS Nano* **2016**, *10* (1), 484–491.
(80) Nie, H.; Li, M.; Li, Q.; Liang, S.; Tan, Y.; Sheng, L.; Shi, W.; Zhang, S. X.-A. Carbon Dots with Continuously Tunable Full-Color Emission and Their Application in Ratiometric PH Sensing. *Chemistry of Materials* **2014**, *26* (10), 3104–3112.
(81) Meng, X.; Chang, Q.; Xue, C.; Yang, J.; Hu, S. Full-Colour Carbon Dots: From Energy-Efficient Synthesis to Concentration-Dependent Photoluminescence Properties. *Chemical Communications* **2017**, *53* (21), 3074–3077.
(82) Grabolle, M.; Spieles, M.; Lesnyak, V.; Gaponik, N.; Eychmüller, A.; Resch-Genger, U. Determination of the Fluorescence Quantum Yield of Quantum Dots: Suitable Procedures and Achievable Uncertainties. *Analytical Chemistry* **2009**, *81* (15), 6285–6294.
(83) Schneider, R.; Weigert, F.; Lesnyak, V.; Leubner, S.; Lorenz, T.; Behnke, T.; Dubavik, A.; Joswig, J.-O.; Resch-Genger, U.; Gaponik, N.; et al. PH and Concentration Dependence of the Optical Properties of Thiol-Capped CdTe Nanocrystals in Water and D2O. *Physical Chemistry Chemical Physics* **2016**, *18* (28), 19083–19092.
(84) Dong, Y.; Pang, H.; Yang, H. Bin; Guo, C.; Shao, J.; Chi, Y.; Li, C. M.; Yu, T. Carbon-Based Dots Co-Doped with Nitrogen and Sulfur for High Quantum Yield and Excitation-Independent Emission. *Angewandte Chemie - International Edition* **2013**, *52* (30), 7800–7804.
(85) Li, D.; Müller, M. B.; Gilje, S.; Kaner, R. B.; Wallace, G. G. Processable Aqueous Dispersions of Graphene Nanosheets. *Nature Nanotechnology* **2008**, *3*, 101.
(86) Perrin, D. D.; Dempsey, B.; Serjeant, E. P. *PKa Prediction for Organic Acids and Bases*; Perrin, D. D., Dempsey, B., Serjeant, E. P., Eds.; Springer Netherlands: Dordrecht, 1981.
(87) Meierhofer, F.; Krieg, L.; Voss, T. GaN Meets Organic: Technologies and Devices Based on Gallium-Nitride/Organic Hybrid Structures. *Semiconductor Science and Technology* **2018**, *33* (8), 83001.

TOC Graphic

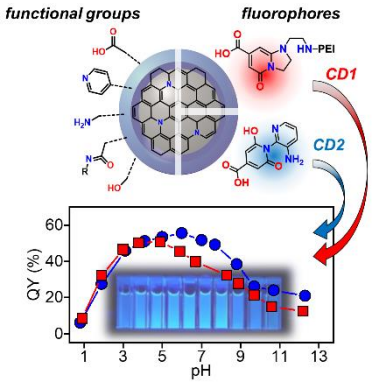
functional groups
fluorophores
HN-PEI
CD1
CD2
QY (%)
pH
0
20
40
60
1
3
5
7
9
11
13